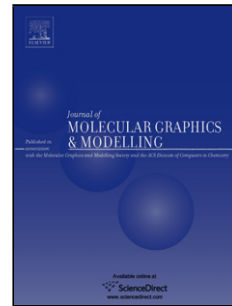


Accepted Manuscript

Title: Structural Basis for Cooperative Binding of Azoles to CYP2E1 as Interpreted through Guided Molecular Dynamics Simulations

Author: Joseph W. Levy Jessica H. Hartman Martin D. Perry
Jr Grover P. Miller



PII: S1093-3263(14)00201-0
DOI: <http://dx.doi.org/doi:10.1016/j.jmgm.2014.11.013>
Reference: JMG 6492

To appear in: *Journal of Molecular Graphics and Modelling*

Received date: 11-8-2014
Revised date: 21-10-2014
Accepted date: 30-11-2014

Please cite this article as: J.W. Levy, J.H. Hartman, M.D.P. Jr, G.P. Miller, Structural Basis for Cooperative Binding of Azoles to CYP2E1 as Interpreted through Guided Molecular Dynamics Simulations, *Journal of Molecular Graphics and Modelling* (2014), <http://dx.doi.org/10.1016/j.jmgm.2014.11.013>

This is a PDF file of an unedited manuscript that has been accepted for publication. As a service to our customers we are providing this early version of the manuscript. The manuscript will undergo copyediting, typesetting, and review of the resulting proof before it is published in its final form. Please note that during the production process errors may be discovered which could affect the content, and all legal disclaimers that apply to the journal pertain.

**Structural Basis for Cooperative Binding of Azoles to CYP2E1 as Interpreted through
Guided Molecular Dynamics Simulations**

Joseph W. Levy^a, Jessica H. Hartman^b, Martin D. Perry Jr^a, and Grover P. Miller^{b,*}

^aDepartment of Chemistry and Physics, Ouachita Baptist University, Arkadelphia, AR

^bDepartment of Biochemistry and Molecular Biology, University of Arkansas for Medical Sciences, Little Rock, AR

*Corresponding Author: Grover P. Miller, Department of Biochemistry and Molecular Biology, University of Arkansas for Medical Sciences, 4301 W Markham St Slot 516, Little Rock, AR 72205, USA; Telephone: 501-526-6486; Email: millergroverp@uams.edu

Running Title: Structural basis for cooperativity between azoles and CYP2E1

Keywords: Cytochrome P450; Allostery; Azole; Molecular Dynamics; Docking; Structure Activity Relationships

Highlights

- Basis for azole cooperativity binding and catalytic inhibition of CYP2E1 is unknown
- Guided Molecular Dynamics simulations yielded 28 CYP2E1-azole complexes
- Active site contacts dominated by common hydrophobic and steric interactions
- Cooperative site interactions are more diverse and dependent on azole structure
- CYP2E1 structure activity relationships revealed challenge to predict cooperativity

Abstract:

CYP2E1 metabolizes a wide array of small, hydrophobic molecules, resulting in their detoxification or activation into carcinogens through Michaelis-Menten as well as cooperative mechanisms. Nevertheless, the molecular determinants for CYP2E1 specificity and metabolic efficiency toward these compounds are still unknown. Herein, we employed computational docking studies coupled to Molecular Dynamics simulations to provide a critical perspective for understanding a structural basis for cooperativity observed for an array of azoles from our previous binding and catalytic studies (Hartman, JH et al (2014) Biochem Pharmacol 87, 523-33). The resulting 28 CYP2E1 complexes in this study revealed a common passageway for azoles that included a hydrophobic steric barrier causing a pause in movement toward the active site. The entrance to the active site acted like a second sieve to restrict access to the inner chamber. Collectively, these interactions impacted the final orientation of azoles reaching the active site and hence could explain differences in their biochemical properties observed in our previous

studies, such as the consequences of methylation at position 5 of the azole ring. The association of a second azole demonstrated significant differences in interactions stabilizing the bound complex than observed for the first binding event. Intermolecular interactions occurred between the two azoles as well as CYP2E1 residue side chains and backbone and involved both hydrophobic contacts and hydrogen bonds. The relative importance of these interactions depended on the structure of the respective azoles indicating the absence of specific defining criteria for binding unlike the well-characterized dominant role of hydrophobicity in active site binding. Consequently, the structure activity relationships described here and elsewhere are necessary to more accurately identify factors impacting the observation and significance of cooperativity in CYP2E1 binding and catalysis toward drugs, dietary compounds, and pollutants.

1. INTRODUCTION

CYP2E1 metabolizes a wide array of biologically important small, hydrophobic molecules (molecular weight < 100) comprised mainly of drugs, dietary compounds, and especially pollutants [1]. Substrates include monocyclic compounds such as styrene, acetaminophen, and isoniazid, as well as bicyclic compounds chlorzoxazone and caffeine. These CYP2E1 substrates undergo oxidation to various metabolites that facilitate their elimination from the human body. Nevertheless, the biological consequences for these events range from detoxification to carcinogen activation [2]. The prediction of these outcomes is hampered by gaps in our knowledge of the molecular determinants for CYP2E1 specificity and metabolic efficiency toward these compounds. Consequently, advances in interpreting and predicting the biological significance of CYP2E1 metabolism requires improvements in our understanding of the mechanisms underlying interactions between CYP2E1 and its substrates.

The Michaelis-Menten mechanism underlies the generally accepted paradigm for CYP2E1 metabolism of substrates and their resulting impact on health outcomes. Nevertheless, growing evidence implicates the importance of more complex cooperative mechanisms for CYP2E1 [3-10]. Those kinetic profiles deviate from the hyperbolic relationship predicted by the Michaelis-Menten mechanism. For 4-nitrophenol, metabolic rates of turnover increase and then decrease as a function of substrate concentration indicating substrate inhibition [3, 6]. Alternatively, many CYP2E1 substrates, including phenacetin, *m*-xylene [5], styrene [7, 8], and 7-ethoxycoumarin, demonstrate a poor efficiency in turnover at low substrate concentrations that rapidly improves at higher concentrations through a positive cooperative mechanism. Recent studies have further

shown that aniline metabolism by CYP2E1 metabolism involves negative cooperativity in which higher substrate concentrations inhibit the ability for the enzyme to reach a maximal rate [9].

While the Hill equation is commonly used to qualify the degree of cooperativity, it reveals nothing of the mechanism underlying the observed kinetic profile. As an alternative, we have identified and validated mechanistic models involving two binding site to explain non-hyperbolic kinetic profiles for CYP2E1 substrates and inhibitors through the use of binding and catalytic experiments coupled with computational structural studies [6-10].

Recently, we investigated the selectivity of both catalytic and cooperative sites for rabbit CYP2E1 through binding and catalytic studies using an array of ten azole inhibitors (Fig. 1) [10]. Data from spectral binding studies for monocyclic azoles were consistent with two binding events, while bicyclic azoles implicated only one. Pyrazole affinity toward the CYP2E1 catalytic site improved upon introduction of a single methyl group at either position 3 or especially 4 of the azole ring. The presence of two methyl groups at positions 3 and 5 precluded any spectral binding event suggesting a lack of interaction with the P450 heme and possibly the catalytic site. A large hydrophobic phenyl ring located at position 3 did not improve pyrazole binding. By contrast, fusion of the pyrazole ring to benzene or cyclohexane greatly increased affinity. The consequences of these binding events on CYP2E1 catalysis were studied through inhibition studies with 4-nitrophenol, a substrate known to bind both sites [6, 11]. Most pyrazoles shared a common mixed cooperative inhibition mechanism in which pyrazole binding rescued CYP2E1 from substrate inhibition. Overall, inhibitor affinities toward the CYP2E1 catalytic site were similar to those reported for binding studies, and the same trend was observed for binding at the cooperative site. Taken together, these studies identified contributions of ring substituents and fusions on the stoichiometry and affinity of azoles for catalytic and cooperative sites;

nevertheless, the complementary role that the CYP2E1 protein structure plays in these interactions remains unknown.

Insights on the function of protein structure have been greatly advanced through computational and X-ray crystallographic methodologies. Initial computational homology models provided the first predictions of CYP2E1 contacts with substrates and inhibitors [12]. The first X-ray crystallographic structures were reported for human CYP2E1 complexes with either 4-methylpyrazole or indazole [13]. These structures validated the importance of amino acid residues in the catalytic site as suggested by computational [12] and site-directed mutagenesis studies [14, 15]. Nevertheless, all crystallographic CYP2E1 structures reported to date include only those with one molecule bound to the enzyme [13, 16, 17], and thus they provide no information on the role of CYP2E1 structure on cooperative interactions.

Computational methods provide a viable solution for identifying CYP2E1 residues responsible for mediating contacts with compounds bound at catalytic and cooperative sites. We were the first to describe docking of 4-nitrophenol, 4-methylpyrazole and indazole to both sites in the binding cavity of rabbit CYP2E1 to explain experimental binding and catalytic data [11]. Subsequent studies by others introduced molecular dynamic simulations to improve predictions of complexes with 4-nitrophenol [18] and aniline [19].

Herein, we employed computational docking studies to identify the structural basis for rabbit CYP2E1 binding and cooperativity toward twelve azoles possessing diverse methyl and ring substituents (Fig. 1). The array of molecules included all azoles from the previously published experimental studies [20] as well as 5-methylpyrazole in order to provide insights on CYP2E1 structure activity relationships relationships. We modeled interactions between these azoles and CYP2E1 through a guided molecular dynamics approach using SYBYL-X 1.3 (Tripos, Inc.).

This technique has been used successfully to find exit channels [21] as well as dock ligands from the outside of the protein to the inner catalytic site [22]. In brief, azoles were initially placed at the entrance of the substrate access channel and were then guided to the binding site. Meanwhile, intermolecular interactions were sampled along the path for the molecule through the protein structure. Complexes were then subjected to multiple cycles of molecular dynamics and energy minimization. When bound at the catalytic site, binary azoles were tethered to the heme iron based on reported Type II binding spectra [6, 10], which in the case of triazoles involved two binding orientations. Taken together, we generated structural solutions for a total of 28 CYP2E1 liganded complexes to understand the cooperative structure activity relationships observed in our previous experimental studies [10].

2. MATERIALS AND METHODS

2.1 Computational Modeling Overview. Sybyl-X 1.3 (Tripos, Inc.) on a Mac workstation was utilized for all molecular modeling, molecular dynamics, MOLCAD surface generator, and analysis. All molecular dynamics simulations used the NTV ensemble [22], and during those efforts, the non-bonding cutoff was set to 12 Å. Minimization of the energy of the protein or liganded complex for CYP2E1 was carried out following the Powell method as implemented in Sybyl software. In addition, PyMOL v1.7 was employed to create all figures depicting the structure of azoles docked to CYP2E1 catalytic and cooperative sites.

2.2 Preparation of Protein and Azoles for Docking. Rabbit CYP2E1 has not been crystallized, and thus a homology model was generated previously [11, 23] and used as a template to generate liganded complexes in this study. The homology model rendered a protein

with twelve major α -helices and four β -sheets, coming together to form the prototypical cytochrome P450 fold (Fig. 2, Panel A). The signature bond between the sulfur atom of Cys437 and the iron of the heme was then added to the structure. Hydrogens were added to the protein based on default values in Sybyl-X 1.3 (Tripos, Inc.) and set to physiological pH. The protonation technique rendered aspartate and glutamate residues in a deprotonated state, while side chain amines were protonated, e.g. lysine. Histidine was set to the neutral δ -tautomer (HID). Gasteiger-Huckel charges were assigned to the atoms except for heme iron, which was assigned a +3 charge to model the state in which azoles bind the heme [24, 25]. The total charge of the protein was then neutralized by the addition of three chloride ions. The resulting protein model was minimized until a 0.05 kcal termination gradient was reached using the Powell method (approximately 2000 iterations). This minimized structure was equilibrated with a molecular dynamics run for 500 fs at 50 K and minimized again prior to docking studies.

For this study, water molecules were not included in the final structure for two reasons. First, active site water molecules were absent in the X-ray crystal structures of CYP2E1 with either 4-methylpyrazole or indazole [26], which was reasonable given the well-characterized hydrophobicity of the CYP2E1 access channel and active site. Second, previous MD simulations on the hydration of P450 active sites demonstrated that the access channel for CYP2E1 was often less than the diameter of a water molecule [27]. This restriction on movement of water and inherent hydrophobicity of the CYP2E1 active site and access channel would minimize the possibility of hydration within the enzyme.

Similarly, Sybyl-X 1.3 (Tripos, Inc.) was used to generate structures for all twelve azole ligands for docking, namely, pyrazole, 3-methylpyrazole, 4-methylpyrazole, 5-methylpyrazole, 3,5-dimethylpyrazole, 3-phenylpyrazole, tetrahydroindazole, indazole, imidazole, benzimidazole,

1,2,3-triazole and benzotriazole (Fig. 1). Gasteiger-Huckel charges were added to the molecules and resulting structures minimized until reaching a 0.05 kcal termination gradient. These structures were then used in docking studies.

2.3 Overall Docking Strategy. We generated CYP2E1 complexes with azoles employing a guided molecular dynamics or guided dock protocol as described by others [22]. The guided molecular dynamics protocol involves applying a force to guide a ligand down the channel during molecular dynamics simulation; however, there was no constraint on the protein scaffold during those simulations. Guided molecular dynamics simulations have been used very successfully in the elucidation of ligand interaction in channels and catalytic sites [21, 22, 28]. When used in our study, the binary complex was initially created through docking of the azole to the active site of CYP2E1. The resulting complex then served as a template to generate ternary complexes that mimic cooperative CYP2E1 complexes. Collectively, these efforts yielded complexes for all twelve azoles docked in this study (Fig. 1).

2.4 Generation of CYP2E1 Complexes through Guided Molecular Dynamics. Simulation of the first binding event for CYP2E1 involved the targeting of the azole to the catalytic site containing the heme moiety during docking. This strategy mimicked the known driving force for their interaction as mediated through the formation of a bond between the sp^2 -hybridized azole nitrogen and the P450 heme iron. Each azole was manually placed at the entrance of the channel near Arg75, Gly101, Glu102 and Val388. The molecule was oriented with the reactive sp^2 -hybridized nitrogen facing the channel entrance as defined and characterized previously [13, 16, 28]. Molecular dynamics was then run on this complex for 2 ps at 50 K with an aggregate between the reactive nitrogen and the heme iron. The aggregate was replaced by a constraint between the two atoms and molecular dynamics run for 200 ps at 50 K. At the completion of this

dynamics simulation, the ligand was always located in the catalytic site, and the complex subjected to an additional molecular dynamics run for 200 ps at 100 K. At the completion of this equilibration of the complex, a bond was manually added between the ligating nitrogen and the heme iron and a final molecular dynamics equilibration run for 200 ps at 100 K. The CYP2E1 binary complex was then minimized. The energy of the resulting binary CYP2E1 complex with the azole was then minimized using the Powell method.

This protocol was the same for all azoles with the exception of the triazoles. These compounds exist as an average of tautomers through resonance; however, computational approaches such as the one used in our study do not lend themselves to incorporating those properties for the triazoles. Rather, we relied on a static tautomer structure and then formed all possible complexes that replicate the necessary iron-nitrogen bond at the active site. For modeling purposes, the liganded nitrogen was depicted as sp^2 , but the remaining two nitrogens were sp^2 and sp^3 even though neither of them possesses true sp^3 character due to resonance. This artifact of the docking process would not likely have a significant impact on possible side chain interactions, given the subtle differences in orientation and partial charge for the hydrogen attached to the nitrogens. These docking possibilities create two different binding orientations and interactions with CYP2E1. Consequently, both bonding possibilities were employed in modeling efforts resulting in two different docking solutions for each triazole. When referring to complexes with either 1,2,3-triazole or benzotriazole, the nitrogen forming the bond with the heme iron will be indicated by the position on the ring after the name as follows: 1,2,3-triazole (N2), 1,2,3-triazole (N3), benzotriazole (N2), and benzotriazole (N3).

Simulation of the second binding event relied on a similar protocol for generating the binary CYP2E1 complex until the step involving the addition of an iron-nitrogen bond. In this case, the

binary CYP2E1 complex served as the docking partner for the second azole. The molecule was placed at the entrance of the substrate access channel and guided into the CYP2E1 binding cavity near the first docked molecule. After the first equilibration dynamics run at 100 K, the structure was minimized and no bond was formed.

3. RESULTS AND DISCUSSION

In this computational study, we leveraged the analysis of 28 individual docked complexes to assess the role of azole structure in binding to rabbit CYP2E1 active and cooperative sites predicted by binding and catalytic inhibition studies [20]. Guided molecular dynamics provided an effective approach to monitor the entrance and movement of each azole down the substrate access channel until docking at the active site (Fig. 2, Panels A and B). The resulting binary complex then served as a template for a docking of the second azole into the cooperative site. After equilibration, there were slight deviations in total energy among the final docked protein-azole complexes (Table S1). The root mean squared (RMSD) for all final protein-azole complexes was below 2 Å (Table S2). Overall, the relatively stable energies and the protein-ligand complex RMSD values indicate that the homology model was sufficiently equilibrated and our docking methods did not contort the overall protein architecture. The collective analysis of these complexes led to critical insights on the favorable and unfavorable interactions between azoles and the residues occurring during the dynamic process of docking to active and cooperative CYP2E1 sites.

3.1. Passage of azole from bulk solvent to the active site

3.2.1. A narrow path to the active site. Azoles traveled down a 22.75 angstrom channel to access the CYP2E1 active site (Fig. 2, Panel B). The maximum width across this channel was 10.00 angstroms and the minimum was 3.75 angstrom based on the van der Waals radii. This spacing imposed steric limitations on passage through the channel and hence impacted movement of azoles toward the active site. The minimal steric bulk for these molecules was the width (6.61 angstroms) and thickness (4.29 angstroms) of the unsubstituted, planar aromatic azoles. More compact ligands could freely rotate within the channel until just prior to reaching the active site; however, larger azoles lacked the ability to freely rotate. The addition of methyl and ring moieties increased the size of the molecules and accordingly limited orientations of molecules through the channel such that molecules never reversed orientation. Consequently, steric clashes between azoles and residues lining the substrate access channel allowed for predominantly small deviations in the path toward the active site. Due to this outcome, the original orientation of the azole entering the channel played an important role in possible docking solutions once the molecule entered the active site.

3.1.2. A pause along the journey to the active site. The ultimate orientation of the molecule depended largely on formation of critical contacts with Leu210 and Leu368, as revealed during molecular dynamics simulations. Within the first 1500 fs, there was a common spike in potential energy between CYP2E1 protein and all azoles (Fig. 3, Panels A and B). The event corresponded to the formation of transient interactions between the azole and Leu210 and Leu368 projecting into the substrate access. The side chain of the leucines mediated van der Waals contacts with azoles prior to the entrance of the active site (Fig. 4, Panels A and B). While all azoles were capable of forming these interactions, the specific points of contact differed among them due to

variations in ring structure, locations of methyl substituents, and presence of a fused ring. Importantly, the transient contact between the leucine residues and azoles influenced their orientations as they traveled down the substrate access channel to the subsequent active site entrance and required conformational changes to allow azoles to pass through the gap toward the active site. This novel role for Leu210 and Leu368 in binding and orientation of the azoles may also come into play with other inhibitors and possibly substrates given the flexibility and propensity to form stabilizing hydrophobic interactions.

3.1.3. Entrance to the active site. Once released from contact with the leucines, azole movement through the channel became restricted at the entrance to the active site by a ring of residues created by Phe207, Ala299, Thr303 and Leu368 (Fig. 4, Panels A and C). The maximum width across this passageway was 6.6 angstroms and the minimum was 4.3 angstrom based on the van der Waals radii. This narrowing of the channel resulted in the free passage of simple unsubstituted monocyclic azoles but hampered movement of substituted azoles. Methyl groups for monocyclic azoles forced the molecules to pass through the active site entrance at certain angles to avoid steric clashes. Notably, these restrictions impacted subsequent formation of an iron-nitrogen bond in the active site, when azoles possessed a methyl group at the C5 position. The fusion of rings for bicyclic azoles resulted in a common and single orientation for molecules entering the active site, which features the sp^3 -hybridized nitrogen oriented towards Thr303. The narrow passageway selected for movement of the azole ring through the entrance first, followed by the additional fused ring. The bicyclic 3-phenylpyrazole was able to completely enter the active site, because the phenyl ring could rotate relative to the pyrazole group and thus be accommodated in the compact CYP2E1 active site (Fig. 4, Panel A and D). In particular, Phe207 played a critical role in these steric clashes, yet mediated stabilizing contacts

with aromatic rings for the azoles. Taken together, the narrow entrance to the active site sterically selected which molecules could enter the active site as well as the possible final binding orientations in the active site.

3.2 Azole docking to the active site

3.2.1. Formation of an iron-nitrogen bond. A hallmark of azole binding to P450s is the formation of an iron-nitrogen bond resulting in a characteristic Type II absorbance difference spectrum [29]. Most of the azoles in this study generated this spectral response, and hence, all azoles were guided to the active site heme iron and a bond created between the appropriate sp^2 nitrogen and heme iron. The introduction of the bond effectively tethered the molecules to protein and through the process led to favorable and unfavorable interactions that could have played a role in their potency as binders or catalytic inhibitors of CYP2E1 [10]. Pyrazoles preferentially oriented with the azole ring perpendicular to the plane of the heme and favored formation of the iron-nitrogen bond with the exception of 5-methyl and 3,5-dimethylpyrazole (Fig. 5). Those latter molecules maximized binding interactions such that they were parallel to the plane of the heme and not poised to interact with the heme iron (Figure 5, Panel C), such that the introduction of an iron-nitrogen bond was necessary to reorient the molecule to be perpendicular to the heme plane (Figure 5, Panel D). This observation could explain the complete absence of a Type II difference spectrum upon titration of CYP2E1 with 3,5-dimethylpyrazole up to 1000 μ M [10]. Interestingly, the larger 3-phenylpyrazole was able to appropriately orient the pyrazole ring for bond formation despite having to tuck the phenyl substituent into the small CYP2E1 active site. For indazole, benzotriazole (N2), and

tetrahydroindazole, the steric restrictions of the active site entrance led to an ideal positioning of the molecules to form the iron-nitrogen bond. This ideal orientation could provide a structural explanation for the high-affinity binding observed for the indazoles through spectral binding and catalytic inhibition studies [10]. The angle of this approach was not ideal for benzimidazole and benzotriazole (N3), whose locations for the sp^2 nitrogens were positioned away from the heme iron. Taken together, most azoles were able to form a stabilizing iron-nitrogen bond consistent with previous binding studies; however, steric clashes played a role in the adoption of orientations most favorable for bond formation.

3.2.2. Orientation of azole in active site toward Thr303. Once ligated to heme iron, the azoles typically favored rotation about the bond to form a stabilizing hydrogen bond to Thr303. Likewise, the side chain of the residue flexes its conformation so that the hydroxyl group provides a suitable hydrogen bond acceptor for the azole hydrogen on the sp^3 nitrogen. This stabilizing interaction was observed for the crystal structures for CYP2E1 with either 4-methylpyraole or indazole bound in the active site [26]. In our computational studies, that hydrogen bond was made for all members of the pyrazole class of molecules except 5-methyl and 3,5-dimethylpyrazole (Fig. 6, Panel A). The methyl group at the C5 position led to steric repulsion with the Thr303 side chain and thus prevented formation of the hydrogen bond as shown in Fig. 6, Panel B. Similarly, the imidazole and triazole classes of compounds were not able to favorably interact with the Thr303 hydroxyl group in 3 of the 6 liganded complexes. Ligation at the 3N sp^2 -hybridized nitrogen positioned the azole hydrogen bond donor towards the entrance of the channel, rather than Thr303. This orientation was observed for both benzimidazole and imidazole. By contrast, both benzotriazole and 1,2,3-triazole successfully formed a hydrogen bond with Thr303, when the iron-nitrogen bond was mediated through the

2N position on the azole. This finding was consistent with the reported crystal structures for CYP2E1 with ω -imidazoyl fatty acids [30] and pilocarpine [17] in which the imidazole ring formed an iron-nitrogen bond but failed to mediate a hydrogen bond within the CYP2E1 active site.

The formation of this hydrogen bond occurs in a very hydrophobic active site and thus could play an important role in the affinity of molecules for CYP2E1. In fact, the strength of this bond may correlate with the affinity of molecules toward CYP2E1. This possibility was recently explored for a structurally diverse array of inhibitors using docking and comparative molecular field analysis (COMFA) [31]. Those efforts demonstrated that inhibitor potency based on IC₅₀ experiments depended on electrostatic interactions between inhibitors and Thr303. In this study, we investigated the structural interactions between an array of azoles and Thr303 as a possible explanation for observed affinities of the molecules for CYP2E1. With the exception of 3,5-dimethylpyrazole, the pyrazole class of molecules demonstrated higher affinities toward CYP2E1 based on our previous binding and catalytic inhibition studies than those observed for the imidazoles or triazoles [10]. These differences in affinity corresponded to computationally docked complexes in this study wherein a hydrogen bond with Thr303 was observed for the high affinity azoles but not for the low affinity azoles. These findings suggest that the formation of a hydrogen bond between azoles and Thr303 in the CYP2E1 active site may provide an additional stabilizing binding contact complementing favorable hydrophobic interactions reported previously [31].

3.2.3. Contacts between azoles and CYP2E1 residues in the active site. After formation of the iron-nitrogen bond, azoles rotated about the bond to form a variety of stabilizing interactions within the active site. The binding space was bordered by a distal ceiling of residues from the

active site entrance, walls from other residues, and a floor by the heme moiety (Fig. 7 Panels A and B). Not surprisingly, active site residues contacting these azoles corresponded to reported Substrate Recognition Sequences (SRS) postulated from sequence alignment studies (Table 1) [32]. The side chains for Ile115, Ala299, Val364, and Leu368 provided stabilizing van der Waals contacts common to all azole complexes (Fig. 7, Panel C). In some cases, these same side chains along with Phe207 and Thr303 created steric clashes for pyrazoles possessing a methyl group at the C5 position after forcing the creation of an iron-nitrogen bond. The binding of bicyclic azoles possessing a fused aromatic ring benefited from pi interactions with Phe207 (Fig. 7, Panel C). The side chain for this residue oriented perpendicular to the aromatic benzyl ring of the azoles to mediate favorable edge-to-face pi contacts. Findings from these computational studies are consistent with our previous photoaffinity labeling experiments [23], site-directed mutagenesis studies [14], and recent publication of crystallographic structures of CYP2E1 complexed with different azoles and fatty acid analogs [17, 26, 30]. Overall, the selectivity of the CYP2E1 active site reflected the passage of the molecule through a restricted active site entrance and subsequent ability to orient perpendicular to the plane of the heme while mediating favorable binding interactions and avoiding steric clashes.

3.3 Azole docking to the cooperative site

3.3.1. Intermolecular interactions between azoles. For all complexes, the second azole docked to a common cooperative site overlapping the active site (Fig. 8). In fact, both bound azoles contacted one another to form a variety of stabilizing intermolecular interactions. Monocyclic pyrazoles favored van der Waals contacts and pi-pi interactions between the

molecules. Pyrazole, 3-methylpyrazole, and 4-methylpyrazole shared a common binding mode in the cooperative site, while steric clashes for 5-methyl and 3,5-dimethylpyrazole forced the molecules into very different orientations relative to other pyrazoles. For the imidazole complex, there were no van der Waals interactions; rather, the two molecules formed a novel stabilizing hydrogen bond between the N3 from the cooperative site imidazole and N1 hydrogen from the active site imidazole (Fig. 8, Panel A). Regardless of the nitrogen involved in heme iron ligation, the active site triazole formed a hydrogen bond between its N1 hydrogen and N2 or N3 on the cooperative site triazole. Even though bicyclic azoles were capable of forming van der Waals contacts, there was a stronger driving force toward pi interactions. All bicyclic azoles in the cooperative site oriented parallel to at least one ring on the active site azole, and thus optimizing binding energy associated with face-to-face pi interactions (Fig. 8, Panel B). The formation of these stabilizing interactions could alter the bond between the azole nitrogen and heme iron in the active site and in doing so, the Type II difference binding spectra. The spectral properties between the CYP2E1 complexes with one or two bound azoles would differ based on that mechanism and thus make it possible to assess the individual binding events as reported for pyrazole, 3-methylpyrazole, and 4-methylpyrazole as well as imidazole [10].

3.3.2. Contacts between azoles and CYP2E1 residues in the cooperative site. The cooperative site derives from residues comprising the active site and its entrance, namely Ile115, Phe207, Ala299, Thr303, Val364, and Leu368, as well as more distal residues unique for this site, i.e. Leu210, Phe298, and Phe478 (Table 2, Fig. 8, Panel C). These residues contacted all azoles in the cooperative site through side chains and the peptide backbone with the exception of Thr303 and Leu368, which were accessible only to the larger bicyclic molecules. These findings are consistent with their location in designated SRSs within the CYP2E1 scaffold [32] and

validated in CYP2E1 crystal structures [17, 26, 30]. For these residues, the hydrophobic side chains contributed predominantly van der Waals contacts to the azoles in this site, but there were exceptions. The occupancy of the cooperative site caused a re-orientation of Phe207 compared to the initial complexes with an azole bound in the active site. The movement of the side chain led to favorable face-to-face pi interactions with monocyclic and bicyclic azoles due to their location in the cooperative site and aromaticity of azole and benzyl rings. Similarly, Phe478 rotated toward the cooperative site to mediate van der Waals contacts through edge-on-edge pi contacts with indazole, benzimidazole, and benzotriazole (N2) but not benzotriazole (N3). The relevance of these side chain contacts to molecules was supported by site-directed mutagenesis studies [14]. Substitution of the Leu368 with valine changed the kinetic mechanism for 4-nitrophenol hydroxylation to positive cooperativity ($n = 1.8$), while substitution of residues more distal from the active site, i.e. Leu210 and Phe478, resulted in a decrease or loss of CYP2E1 activity. These findings underscore the role of hydrophobic contacts in the cooperative site and potential contributions to CYP2E1 metabolism.

Variations in the azole binding modes also led to hydrogen bonds forming between their respective hydrogens on the sp^3 nitrogen and peptide backbone for different residues. The azole ring mostly overlaid for pyrazole, 3-methylpyrazole, 4-methylpyrazole, and 3-phenylpyrazole such that all molecules formed a contact to the peptide backbone of Phe298 (Fig. 8, Panel D). Triazole (N3) made a similar hydrogen bond to the peptide backbone of Phe478, while the same type of bond for benzotriazole (N3) was toward Ala299. Lastly, the peptide backbone for Leu210 mediated a hydrogen bond to the amino hydrogen of imidazole and tetrahydroindazole. The relevance of these interactions would be difficult to assess using typical site-directed mutagenesis approaches due to the limitation of changes in only side chains for the residues.

Taken together, the binding space of the cooperative site led to the adoption of a greater variety of binding modes and types of interactions between CYP2E1 residues and azoles than observed for the active site. Insights gained on cooperative site binding provide an important foundation for understanding the selectivity of the interactions and the resulting consequences on CYP2E1 binding and catalysis.

Concluding Remarks

We employed computational docking studies coupled to Molecular Dynamics simulations to provide a critical perspective for understanding a structural basis for cooperativity observed for an array of azoles from our previous binding and catalytic studies [10]. The resulting 28 CYP2E1 complexes revealed a common passageway for azoles that included a hydrophobic steric barrier causing a pause in movement toward the active site. The entrance to the active site acted like a second sieve to restrict access to the inner chamber. Collectively, these interactions impacted the final orientation of azoles reaching the active site and hence could explain differences in their biochemical properties observed in our previous studies, such as the consequences of methylation at position 5 of the azole ring. The cooperative association of a second azole demonstrated significant differences in interactions stabilizing the bound complex than observed for the first binding event. Intermolecular interactions occurred between the two azoles as well as CYP2E1 residue side chains and backbone and involved both hydrophobic contacts and hydrogen bonds. The relative importance of these interactions depended on the structure of the respective azoles indicating the absence of specific defining criteria for binding unlike the well-characterized dominant role of hydrophobicity in active site binding. Consequently, the structure

activity relationships described here and previously by us [10] and others [31] are necessary to more accurately identify factors impacting the observation and significance of cooperativity in CYP2E1 binding and catalysis toward drugs, dietary compounds, and pollutants.

Acknowledgements

Support for this publication was provided in part by the Arkansas INBRE program, through a grant from the National Institutes of Health (NIH) National Institute of General Medical Sciences (NIGMS) (P20 GM103429) (formerly P20RR016460) (JWL, MDP, and GPM) as well as the Ouachita Baptist University Patterson Summer Science Program (JWL). Additional support derived from an NSF Fellowship awarded to JHH (DGE 1452779).

References

1. Miller, G.P., *Advances in the Interpretation and Prediction of CYP2E1 Metabolism from a Biochemical Perspective*. Expert Opin Drug Metab Toxicol, 2008. **4**(8): p. 1053-64.
2. Trafalis, D.T., et al., *CYP2E1 and risk of chemically mediated cancers*. Expert Opin Drug Metab Toxicol. **6**(3): p. 307-319.
3. Koop, D.R., *Hydroxylation of p-nitrophenol by rabbit ethanol-inducible cytochrome P-450 isozyme 3a*. Mol Pharmacol, 1986. **29**: p. 399-404.
4. Hargreaves, M.B., et al., *Inhibition of p-nitrophenol hydroxylase in rat liver microsomes by small aromatic and heterocyclic molecules*. Drug Metab Dispos, 1994. **22**: p. 806-810.
5. Harrelson, J.P., W.M. Atkins, and S.D. Nelson, *Multiple-Ligand Binding in CYP2A6: Probing Mechanisms of Cytochrome P450 Cooperativity by Assessing Substrate Dynamics*. Biochemistry, 2008. **47**(9): p. 2978-2988.
6. Collom, S.L., et al., *CYP2E1 substrate inhibition: Mechanistic interpretation through an effector site for monocyclic compounds*. J Biol Chem, 2008. **283**(6): p. 3487-3496.
7. Hartman, J.H., G. Boysen, and G.P. Miller, *CYP2E1 Metabolism of Styrene Involves Allostery*. Drug Metab Dispos, 2012. **40**(10): p. 1976-1983.
8. Hartman, J.H., G. Boysen, and G.P. Miller, *Cooperative effects for CYP2E1 differ between styrene and its metabolites*. Xenobiotica, 2013. **43**(9): p. 755-64.
9. Hartman, J.H., K. Knott, and G.P. Miller, *CYP2E1 hydroxylation of aniline involves negative cooperativity*. Biochem Pharmacol, 2014. **87**(3): p. 523-33.

10. Hartman, J.H., et al., *Structure of pyrazole derivatives impact their affinity, stoichiometry, and cooperative interactions for CYP2E1 complexes*. Arch Biochem Biophys, 2013. **537**(1): p. 12-20.
11. Collom, S.L., et al., *CYP2E1 substrate inhibition. Mechanistic interpretation through an effector site for monocyclic compounds*. J Biol Chem, 2008. **283**(6): p. 3487-96.
12. Park, J.Y. and D. Harris, *Construction and Assessment of Models of CYP2E1: Predictions of Metabolism from Docking, Molecular Dynamics, and Density Functional Theoretical Calculations*. J Med Chem, 2003. **46**(9): p. 1645-1660.
13. Porubsky, P.R., K.M. Meneely, and E.E. Scott, *Structures of human cytochrome P-450 2E1. Insights into the binding of inhibitors and both small molecular weight and fatty acid substrates*. J Biol Chem, 2008. **283**(48): p. 33698-707.
14. Spatzenegger, M., et al., *Analysis of Differential Substrate Selectivities of CYP2B6 and CYP2E1 by Site-Directed Mutagenesis and Molecular Modeling*. J Pharmacol Exp Ther, 2003. **304**(1): p. 477-487.
15. Porter, T.D., *Mutagenesis at a highly conserved phenylalanine in cytochrome P450 2E1 affects heme incorporation and catalytic activity*. Biochemistry, 1994. **33**: p. 5942-5946.
16. Porubsky, P.R., K.P. Battaile, and E.E. Scott, *Human cytochrome P450 2E1 structures with fatty acid analogs reveal a previously unobserved binding mode*. J Biol Chem, 2010. **285**(29): p. 22282-90.
17. DeVore, N.M., et al., *Structural comparison of cytochromes P450 2A6, 2A13, and 2E1 with pilocarpine*. FEBS J, 2012. **279**(9): p. 1621-1631.
18. Liu, Y., et al., *$\pi-\pi$ Stacking mediated drug-drug interactions in human CYP2E1*. Proteins: Struct, Funct, Bioinf, 2013. **81**(6): p. 945-954.

19. Li, J., et al., *A negative cooperativity mechanism of human CYP2E1 inferred from molecular dynamics simulations and free energy calculations*. J Chem Inf Model, 2011. **51**(12): p. 3217-25.
20. Hartman, J.H., et al., *Structure of Pyrazole Derivatives Impact their Affinity, Stoichiometry, and Cooperative Interactions for CYP2E1 Complexes*. Arch Biochem Biophys, 2013.
21. Shen, Z., et al., *Investigation of Indazole Unbinding Pathways in CYP2E1 by Molecular Dynamics Simulations*. PLoS ONE, 2012. **7**(3).
22. Lafite, P., et al., *Unusual Regioselectivity and Active Site Topology of Human Cytochrome P450 2J2*. Biochemistry, 2007. **46**(36): p. 10237-10247.
23. Collom, S.L., Jamakhandi, A.P., Tackett, A.J., Radominska-Pandya, A., Miller, G.P., *CYP2E1 Active Site Residues in Substrate Recognition Sequence 5 Identified by Photoaffinity Labeling and Homology Modeling*. Arch Biochem Biophys, 2007. **459**(1): p. 59-69.
24. Meunier, B., S.P. Visser, and S. Shaik, *Mechanism of Oxidation Reactions Catalyzed by Cytochrome P450 Enzymes*. Chem Rev, 2004. **104**: p. 3947-3980.
25. Jensen, K.P. and U. Ryde, *How O₂ binds to heme: reasons for rapid binding and spin inversion*. J Biol Chem, 2004. **279**(15): p. 14561-9.
26. Porubsky, P.R., K.M. Meneely, and E.E. Scott, *Structures of Human Cytochrome P-450 2E1: Insights into the binding of inhibitors and both small molecular weight and fatty acid substrates*. J. Biol. Chem., 2008. **283**(48): p. 33698-33707.

27. Hendrychova, T., Berka, K, Navratilova, V, Anzenbacher, P, Otyepka, M, *Dynamics and hydration of the active sites of mammalian cytochromes P450 probed by molecular dynamics simulations*. Curr Drug Metab, 2012. **13**(2): p. 177-89.
28. Fishelovitch, D., et al., *Theoretical Characterization of Substrate Access/Exit Channels in the Human Cytochrome P450 3A4 Enzyme: Involvement of Phenylalanine Residues in the Gating Mechanism*. J Phys Chem B, 2009. **113**: p. 13018-13025.
29. Schenkman, J.B., H. Remmer, and R.W. Estabrook, *Spectral studies of drug interaction with hepatic microsomal cytochrome P-450*. Mol Pharmacol, 1967. **3**: p. 113-123.
30. Porubsky, P.R., K.P. Battaile, and E.E. Scott, *Human Cytochrome P450 2E1 Structures with Fatty Acid Analogs Reveal a Previously Unobserved Binding Mode*. J Biol Chem, 2010. **285**(29): p. 22282-22290.
31. Martikainen, L.E., et al., *Interactions of inhibitor molecules with the human CYP2E1 enzyme active site*. Eur J Pharm Sci, 2012. **47**(5): p. 996-1005.
32. Gotoh, O., *Substrate recognition sites in cytochrome P450 family 2 (CYP2) proteins inferred from comparative analysis of amino acid and coding nucleotide sequences*. J Biol Chem, 1992. **267**: p. 83-90.

Tables**Table 1: Amino acid residues contacting azoles bound to the CYP2E1 active site**

Residue	SRS^a	Structural element	Source of contact	Type of contact
Ile115	1	B-C Loop	side chain	van der Waals
Phe207	2	F helix	side chain	edge-to-face pi contacts
Ala299	4	I helix	side chain	van der Waals
Thr303	4	I helix	side chain hydroxyl group	hydrogen bond
Val364	5	K-L Loop	side chain	van der Waals
Leu368	5	K-L Loop	side chain	van der Waals

^aSRS, substrate recognition sequences, as defined by Gotoh [32].

Table 2: Amino acid residues contacting azoles bound to the CYP2E1 cooperative site

Residue	SRS^a	Structural element	Source of contact	Type of contact
Ile115	1	B-C Loop	side chain	van der Waals
Phe207	2	F helix	side chain	face-to-face pi contacts
Leu210	(2) ^b	F helix	peptide backbone side chain	hydrogen bond van der Waals
Phe298	4	I helix	peptide backbone side chain	hydrogen bond van der Waals
Ala299	4	I helix	peptide backbone side chain	hydrogen bond van der Waals
Thr303	4	I helix	side chain hydroxyl group	hydrogen bond
Leu368	5	K-L Loop	side chain	van der Waals
Phe478	6	L-C terminus Loop	peptide backbone side chain	hydrogen bond van der Waals

^aSRS, substrate recognition sequences, as defined by Gotoh [32].

^bResidue lies adjacent to indicated SRS

Figure Legends:

Figure 1. Azoles used for computational docking to CYP2E1 active and cooperative sites.

Figure 2. Overall architecture of CYP2E1. (A) Structure of equilibrated CYP2E1 structure used in the docking studies in which alpha helices are indicated by letter designations. (B) In these studies, molecules interact with three distinct areas of CYP2E1 structure, namely, the access channel, cooperative site, and active site.

Figure 3. Transient intermediate formed between CYP2E1 and azoles during Molecular Dynamics simulations. At 1000 fs, there was a common spike in potential energy during the first docking event for all (A) pyrazoles and (B) other azoles.

Figure 4. Impact of sterics on azoles entering the active site. (A) A cross section of the channel showing a sterically constricted site in the channel, the sterically constricted entrance to the active site, and the active site. (B) Leu210 (blue) and Leu368 (dark blue) form a constriction in the active site channel that mediates stabilizing contacts as shown for 3-phenylpyrazole (green). This action causes a spike in potential energy as azoles travel toward the active site (see Fig. 3) (C) The entrance to the active site involves another constriction in the channel created by Leu368, Val364, Phe207 and Ala299. (D) The last ring of residues defines the final contacts mediated through the active site.

Figure 5. Impact of iron-nitrogen bond formation on azole orientation. (A) Final equilibrated position of pyrazole prior to formation of the iron nitrogen bond, whereby azole is perpendicular to the plane of the heme. (B) Pyrazole following formation of the iron-nitrogen bond and equilibration showing little change in orientation. (C) Final equilibrated position of 3,5-dimethylpyrazole prior to formation of iron-nitrogen bond, whereby azole is parallel to the plane of the heme due to steric clashes. (D) Reorientation of 3,5-dimethylpyrazole relative to heme following formation of the iron-nitrogen bond and equilibration.

Figure 6. Hydrogen bond formation observed for most, but not all CYP2E1-azole complexes. (A) Most azoles preferentially formed a hydrogen bond between an sp^3 -hybridized nitrogen on the azole ring and hydroxyl group from the Thr303 side chain. (B) The presence of a methyl group at the C5 position precluded formation of the hydrogen bond due to steric clashes with the Thr303 side chain as represented for the 5-methylpyrrole and 3,5-dimethylpyrazole complexes.

Figure 7. The CYP2E1 active site. (A) The CYP2E1 active site is a box bordered by the floor comprised of the heme moiety, walls by Ile115, Phe298, Ala299, Thr303, Val364 and Leu368, and ceiling by Phe207 and Leu210. (B) Monocyclic azoles in the figure, formed substantial van der Waals contacts with residues lining the active site as shown for pyrazole. (C) Bicyclic azoles, like benzimidazole (N2), formed similar active site contacts as observed for monocyclic azoles with the addition of significant face-to-edge pi interactions with Phe207.

Figure 8. The CYP2E1 cooperative site. The association of a second azole to CYP2E1 led to significant intermolecular interactions including hydrogen bond formation and pi interactions, such that the active and cooperative sites communicated through bound azoles as shown for (A) imidazole and (B) benzotriazole (N2). (C) The extent of interactions at the cooperative site is best shown by contacts mediated by the second, bound indazole molecule to Ile115, Phe207, Leu210, Phe298, Ala299, Leu368 and Phe478. (D) In addition to pi interactions and van der Waals interactions, several monocyclic azoles, e.g. pyrazole (shown in the figure), formed a stabilizing hydrogen bond with the carbonyl backbone of Phe298.

Figure 1

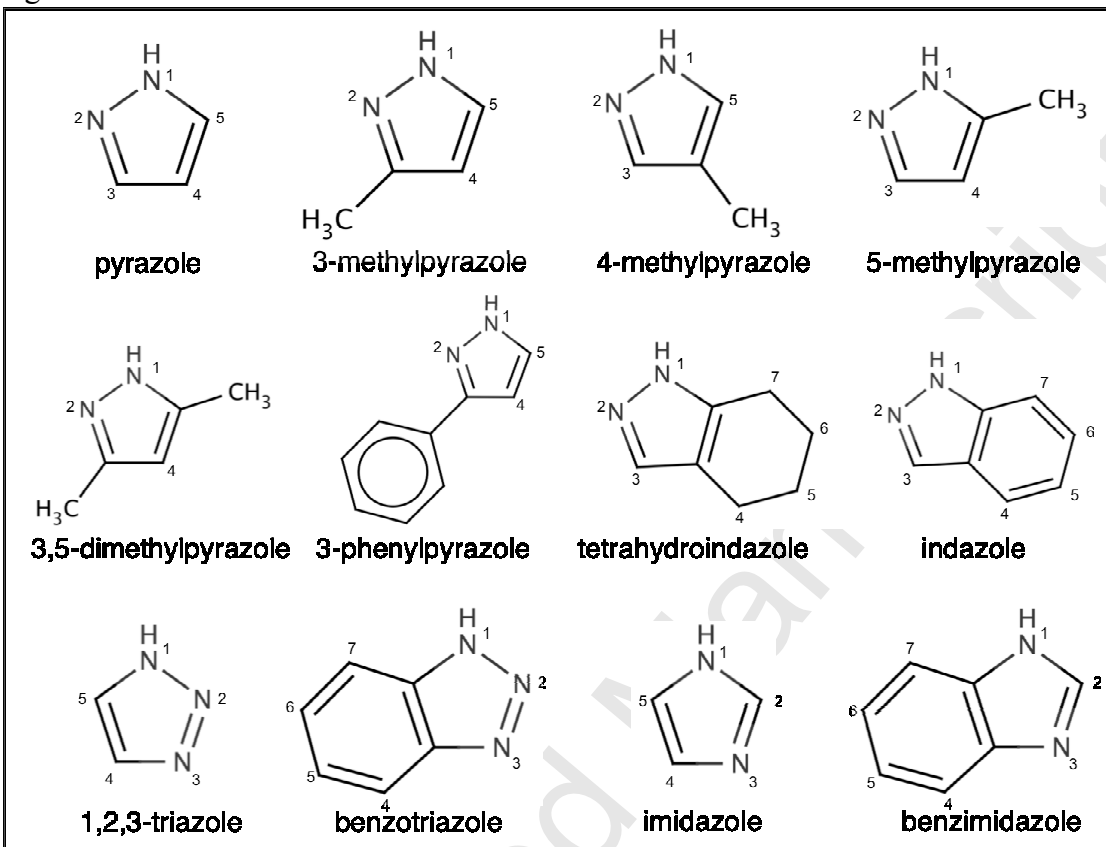


Figure 2

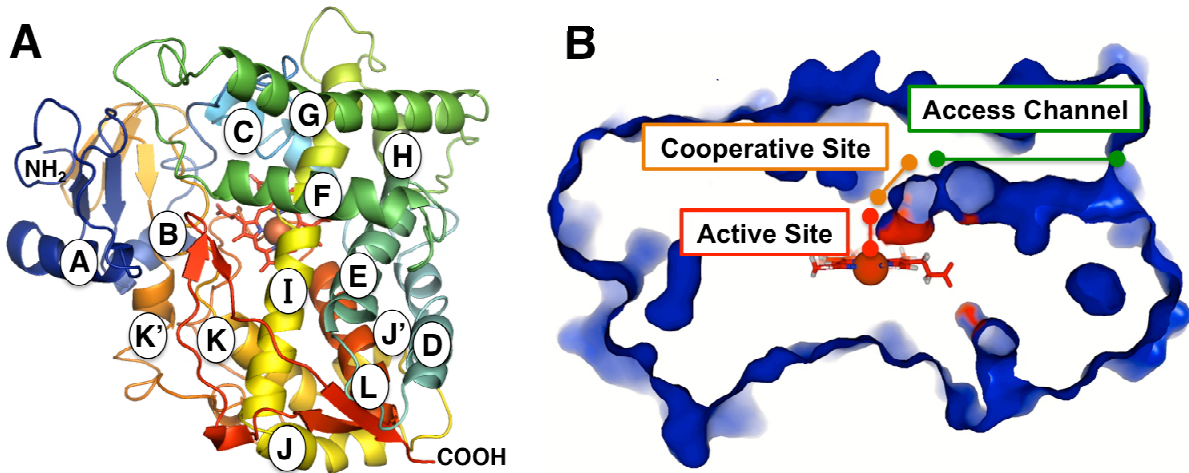


Figure 3

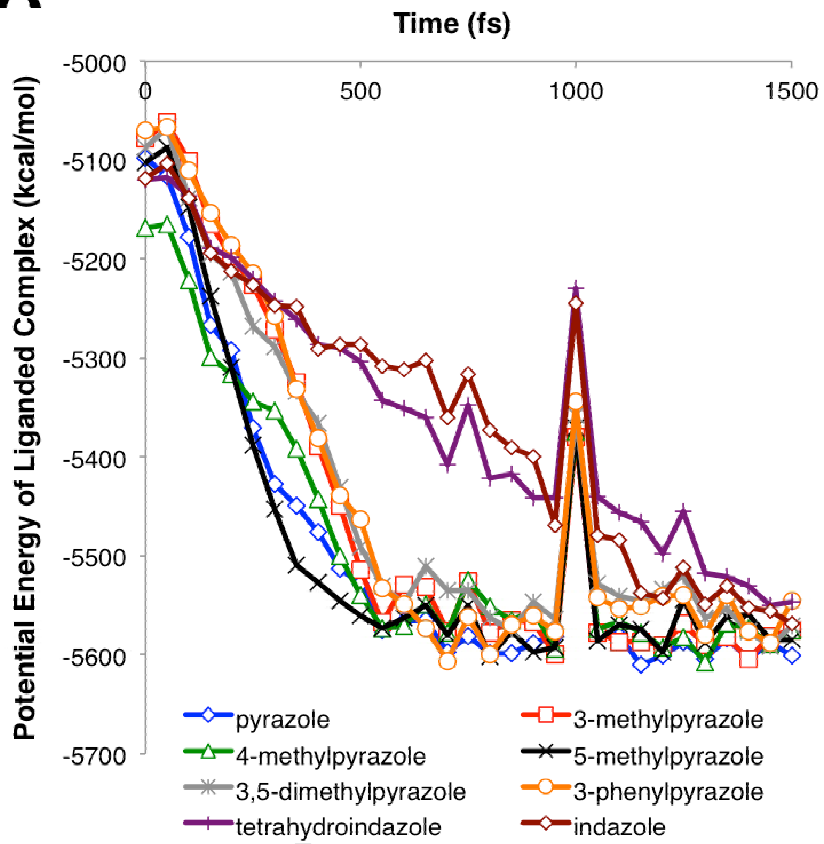
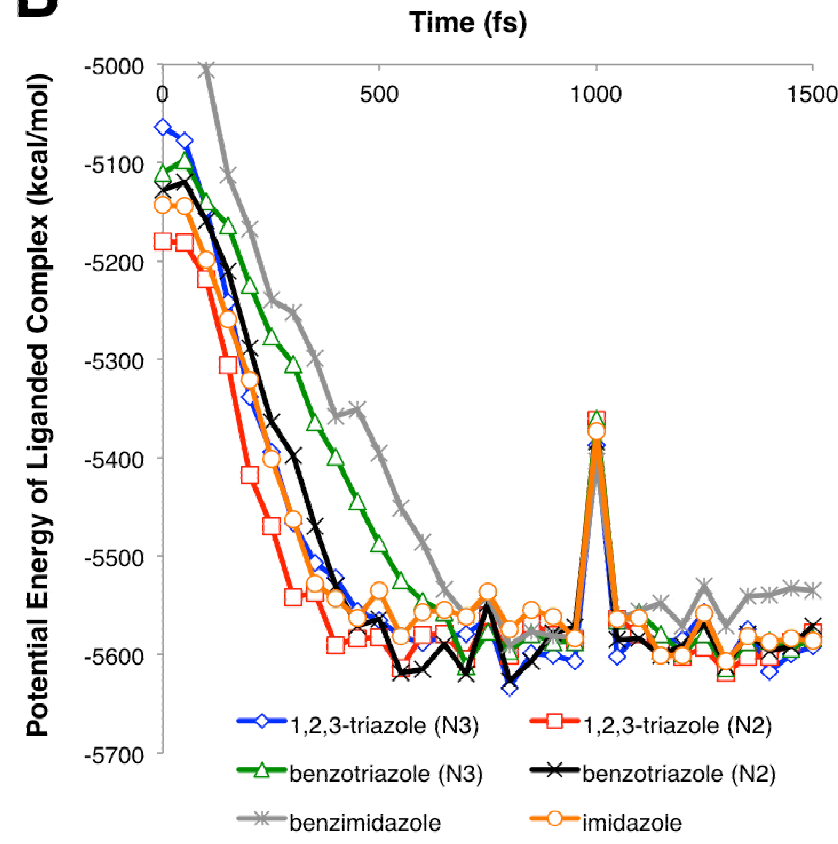
A**B**

Figure 4

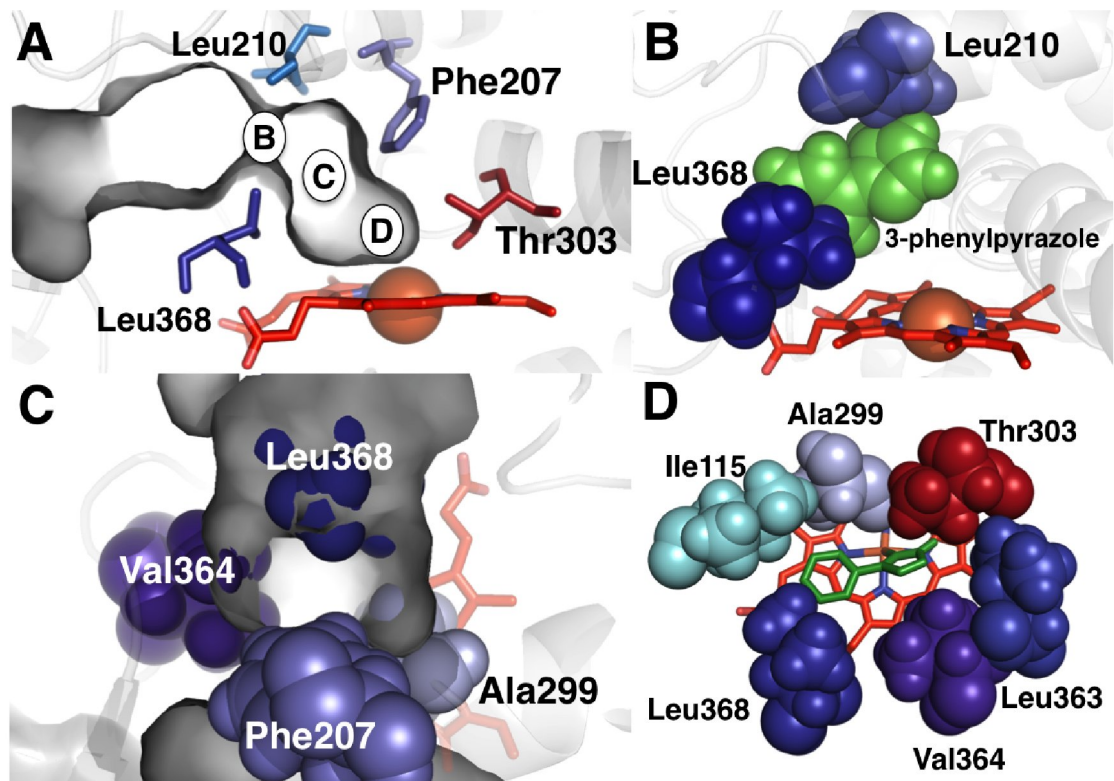


Figure 5

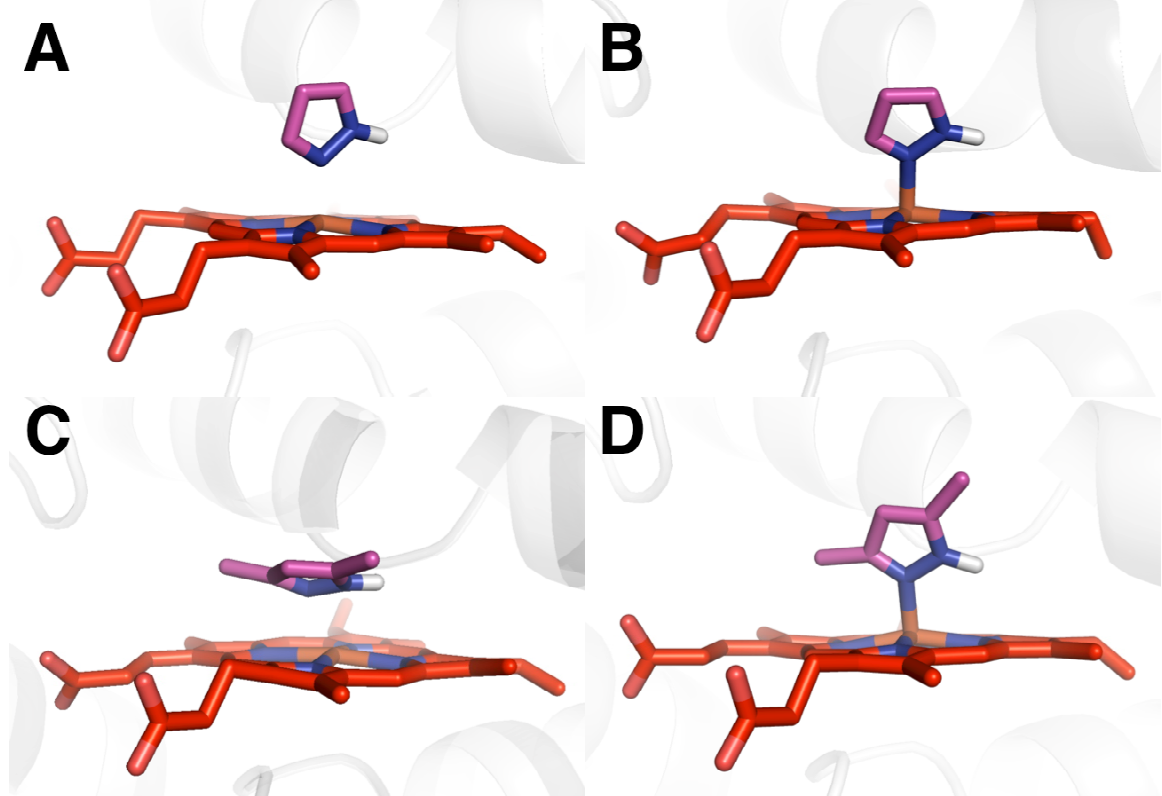


Figure 6

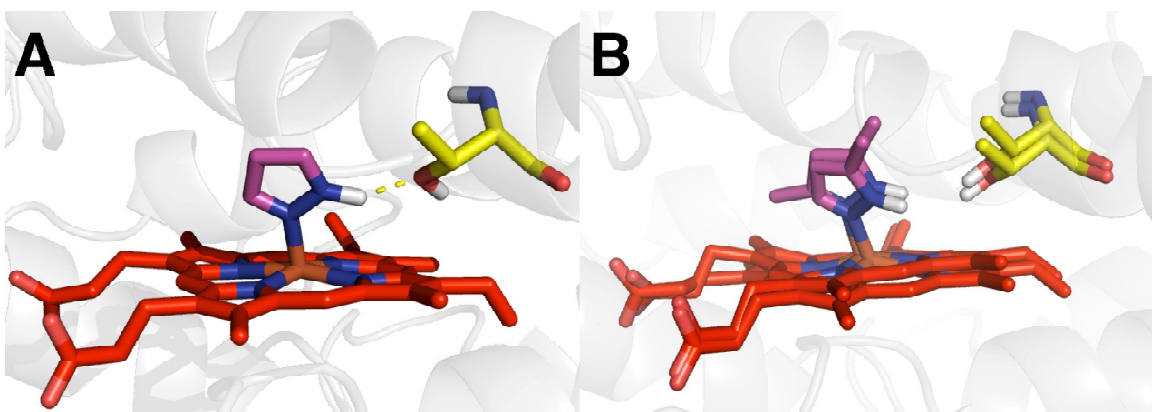


Figure 7

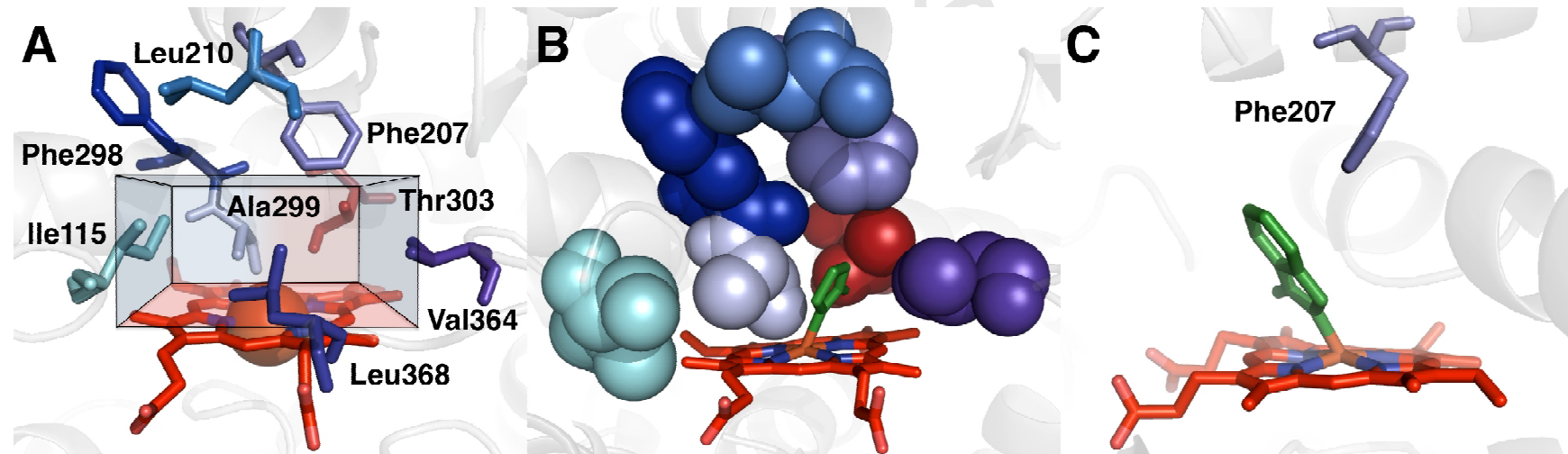


Figure 8

